Received: 27 September 2022 | Revised: 14 March 2023 | Accepted: 3 April 2023

DOI: 10.1002/nag.3542

RESEARCH ARTICLE

WILEY

A new method for the analysis of foundation behavior in sand under drained high-cycle loading

Shuhan Cao | **Khalid Abdel-Rahman** | **Martin Achmus**

Institute for Geotechnical Engineering, Leibniz University Hannover, Hannover, Niedersachsen, Germany

Correspondence
Khalid Abdel-Rahman, Institute for Geotechnical Engineering, Leibniz University Hannover, Hannover, Niedersachsen, 30167, Germany.Email: khalid@igth.uni-hannover.de

Abstract

In offshore technology, especially in offshore wind energy converters, permanent deformations of the structures must be limited. For that purpose, the accumulation of permanent deformation due to cyclic loading must be predicted as accurately as possible. To account for this accumulation in non-cohesive soils, different approaches such as semi-empirical methods, p-y curve methods and numerical methods are available. Among the numerical approaches, the Stiffness Degradation Method (SDM) has the advantage of practical feasibility. However, it is only compatible with a relatively simple constitutive law and does not consider the influence of un- and reloading stress paths in the soil. With the basic concept of SDM, a new method termed Cyclic Strain Accumulation Method (CSAM) is proposed. In CSAM, the weaknesses of SDM, especially its incompatibility with advanced constitutive laws, are overcome, while retaining the practical feasibility as the main advantage of SDM. Through numerical calculations of a monopile, it is found that the CSAM is able to reproduce SDM results if the same material law is applied. The results of SDM and CSAM for the case of a vertical loaded strip footing have been presented. The comparison shows that the CSAM results are more realistic than the SDM results. Besides, CSAM is computationally more efficient and open for further optimisation. The effects of sophisticated material law and the consideration of un- and reloading are investigated. Results show that CSAM is a promising new approach to account for the deformation of foundations under cyclic loading in non-cohesive soils.

KEYWORDS

cyclic deformation, cyclic strain accumulation method (CSAM), finite element method (FEM), monopile, offshore wind energy converter, stiffness degradation method (SDM)

1 | INTRODUCTION

During its design lifetime, offshore wind energy converters (OWECs) are subjected to a high number of cyclic loads resulting from winds and waves, thus undergoing increasing permanent deformations of the foundation structure. These cyclic loads are of special relevance because the vertical loads, which for usual offshore structures govern the design, are small relative to the eccentric loads caused by the large lever arm between the nacelle and mudline. With regard to serviceability,

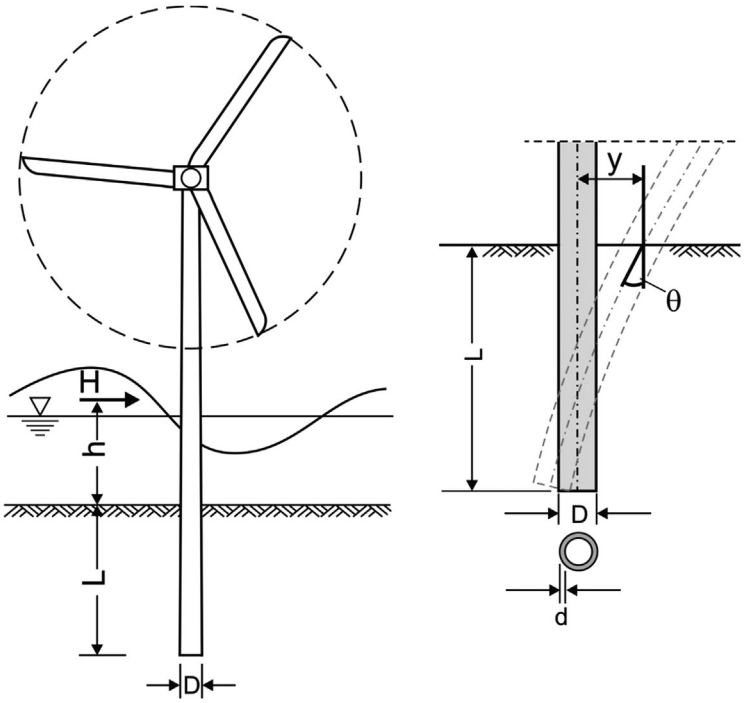

FIGURE 1 System of offshore wind energy converter founded on a monopile.

it is often required in offshore wind projects that the permanent rotation of the foundation structure shall be limited to 0.5°, including an installation tolerance of 0.25°, which means that the additional accumulated rotation due to lateral cyclic loading must be limited to less than 0.25°. Therefore, predicting the permanent deformation and rotation due to cyclic eccentric loads is greatly important (Figure 1).

Under proper water depth and subsoil conditions, the foundations for OWECs are often built in the form of monopiles. In the practical design of monopiles, the cyclic deformation is often estimated using semi-empirical equations derived from small-scale experiments in terms of head displacement or head rotation. These approaches are simple for the application, but their weaknesses are that they do not consider site-specific conditions, which the so-called cyclic p-y curve approaches addressed. In the cyclic p-y curve approaches, the pile is treated as a beam and the soil structure interaction is described through non-linear springs, with the soil contribution considered only in an integrated sense. This simplification also makes the accuracy of p-y curve methods inherently limited.

These weaknesses are overcome using numerical approaches that distinguish between implicit and explicit methods of cyclic deformation. The implicit method is an extension of classical plasticity theory in that the real load scenario, that is, every single loading cycle, is followed in the numerical model, and the cyclic deformation is computed based on the plasticity theory. A typical example of a material law applied here is the SANI-Sand model after Dafalias et al. and Liu et al.[1,2] Since the exact loading scenario is followed and computed, the implicit method is computationally costly and can normally only be applied for a low number of cycles (maximal up to several hundred), as for large cycle numbers, the numerical errors become too great and make the system difficult to converge. In practical cases, however, it is often required to compute the cyclic deformation after millions of cycles. In this sense, it may not be possible to utilise the implicit method, but only the explicit method. The explicit method, in contrast, does not concentrate on a single loading cycle. Here the mechanical effect of cyclic loading, that is, the cyclic deformation of a given cycle number, is computed directly through the accumulation laws derived from cyclic laboratory element tests (such as cyclic triaxial tests) with the assumption that the stress state keeps basically unchanged during the cyclic loading. In this way, numerical simulation to a high cycle number is possible. Examples of explicit methods are High-Cycle Accumulation Method (HCA) after Wichtmann et al. and Niemunis et al.[3,4] and the Stiffness Degradation Method (SDM) after Achmus et al.[5]

In the HCA model, a hypoplastic material law is applied and the strain accumulation due to cyclic loading of a soil element is determined by an equation considering load history, strain amplitude, void ratio, confining pressure, stress ratio and load cycle number. In the numerical simulation, the accumulated strain is considered as pseudo-creep strain. The method is capable to deal with general cyclic loading conditions, but the simulation is complex and a large number of cyclic soil tests is necessary to identify the numerous input parameters.

In the Stiffness Degradation Method (SDM) (Achmus et al.[5]), the cyclic deformation is generated by applying the results of cyclic triaxial tests through the degradation of elastic soil stiffness specifically, depending on the cycle number and local load intensity, as detailed in Section 2.2. An important advantage of SDM is its practical feasibility compared to other more rigorous numerical methods such as SANI-Sand and High Cycle Accumulation (HCA) methods. The SDM is built based on the elasto-plastic constitutive law, Mohr-Coulomb's perfect plasticity, whose parameters can be estimated through well-known empirical values and whose cyclic soil behaviour is described through only two regression parameters derived from cyclic triaxial testing. Several studies and comparisons with experimental data showed that it is possible to achieve a realistic estimation of the cyclic behaviour of monopiles through the SDM (see Achmus et al.,[5] Albiker,[6] Westermann et al.,[7,8] and Yang et al.[9]). However, a disadvantage of SDM is that the conceptual approach of elastic stiffness degradation requires using a simple material law with elastic stiffness, in which the elastic deformation shall be decisive: the elasto-plastic constitutive law with perfect plasticity. A more accurate characterisation of the soil behaviour by an advanced material law is thus impossible within the framework of the SDM. The numerical degradation procedure in soil stiffness also indicates that SDM can only be used for the monopile under horizontal loading. If, as in the case of a gravity foundation, the cyclic vertical deformations are to be investigated, the degradation of the soil stiffness not only leads to an increase in deformation as a result of cyclic loads, but also as a result of permanent (gravity) loads.

Another inaccuracy of the SDM lies in the fact that the material law does not distinguish between the primary loading and reloading path. Hence, the stress state of the soil element, which serves as the basis for the explicit method, can only be determined from the primary loading path in the system. In fact, the stress state in a load cycle is more representative by considering the unloading and reloading path of the system.

In this paper, a new method termed 'Cyclic Strain Accumulation Method (CSAM)' is presented in which accumulated strains derived from cyclic tests are applied directly (instead of indirectly via stiffness degradation) in the numerical model. The CSAM adopts essential aspects of the SDM but allows the consideration of more advanced material models. In the comparison computations, the CSAM results are compared with the SDM results using the same constitutive law as the SDM. Furthermore, the CSAM is applied with a more sophisticated constitutive law, viz. Hypoplasticity, to investigate the influence of material law and of un- and reloading stress path on cyclic accumulation behaviour of the monopile.

2 | CURRENT DESIGN METHODS FOR LATERALLY LOADED MONOPILES

As already mentioned, the cyclic behaviour of laterally loaded monopiles can be described through semi-empirical approaches, cyclic p-y curves, and numerical methods. In the following, these methods are described briefly.

2.1 | The semi-empirical approaches and p-y curve methods

Typical semi-empirical approaches, as summarised in Table 1 (taken from[10]), describe an increase of cyclic deformation relative to the deformation after the first loading in terms of pile head displacement or rotation. These approaches are derived from various experiment conditions; thus, they have a wide range of fitting parameters. Consequently, quantifying the cyclic behaviour through semi-empirical approaches is difficult, as the site-specific conditions, such as subsoil conditions and actual soil pile interaction, are not taken into account.

The cyclic p-y curves of non-cohesive soils are often derived by modifying static p-y curves. In the cyclic approach after API (American Petroleum Institute),[11] the cyclic p-y curve is expressed as:

$$p = A \cdot p_u \cdot \tanh\left(\frac{k \cdot z}{A \cdot p_u} \cdot y\right) \tag{1}$$

In this equation, p_u is the ultimate resistance depending on depth z and friction angle φ of the soil; k is a stiffness parameter also depending on φ. The calibration factor A shall be set to A = 0.9 for the case of cyclic loading. It is usually assumed that this factor applies to a cycle number of N ≈ 100 (cf.[12]).

Based on this concept, Dührkop (2009)[12] proposed a modified formula based on small-scale 1 g test:

$$p = \tilde{A}_{cyc} \cdot p_u \cdot \tanh\left(\frac{k \cdot z}{0.9 \cdot p_u} \cdot y\right) \tag{2}$$

TABLE 1 Overview of models for cyclic displacement or rotation accumulation resulting from lateral cyclic loading.[10].

Reference	Model	Test type	Load cycles	Pile-soil-system	Model parameters
Peralta (2010)	$y_N = y_1 \cdot N^{\alpha_P}$ $y_N = y_1 \cdot (1 + t_P \cdot \ln N)$	1 g 13 static 21 cyclic	10,000	D = 6 cm L/D = 3.33-8.33 h = 240 mm = const. D_r = 0.45 & 0.65	Rigid piles: $\alpha_P = 0.12$ Flexible piles: $t_P = 0.21$
LeBlanc et al. (2010a)	$\theta_N = \theta_1 \cdot (1 + T_{b,LB} \cdot T_{c,LB} \cdot N^{\alpha_{\theta,LB}})$	1 g 6 static 15 cyclic	7,400–65,370	D = 8 cm L/D = 4.5 = const. h/D = 5.38 = const. D_r = 0.04 & 0.38	$\alpha_{LB} = 0.31$ $T_{b,LB}(\zeta_b, D_r = 0.38) = 0.414\,\zeta_b - 0.023$[a] $T_{b,LB}(\zeta_b, D_r = 0.04) = 0.303\,\zeta_b - 0.044$ $T_{c,LB}(\zeta_c) = a\,\zeta_c^4 + b\,\zeta_c^3 + c\,\zeta_c^2 + d\,\zeta_c + e$[b]
Klinkvort & Hededal (2013)	$y_N = y_1 \cdot N^{T_{b,K\&H} \cdot T_{c,K\&H}}$	Centrifuge 5 static 12 cyclic	250–10,000	D = 2.8 cm & 4.0 cm L/D = 6 = const. h/D = 15 = const. D_r = 0.79 - 0.96	$T_{b,K\&H}(\zeta_b) = 0.61\,\zeta_b - 0.013$ $T_{c,K\&H}(\zeta_c) = (\zeta_c + 0.63)(\zeta_c - 1)(\zeta_c - 1.64)$
Li et al. (2015)	$y_N = y_1 \cdot N^{\alpha_{y,L}}$ $y_N = y_1 \cdot (1 + t_{y,L} \cdot \ln N)$ $\theta_N = \theta_1 \cdot N^{\alpha_{\theta,L}}$ $\theta_N = \theta_1 \cdot (1 + t_{\theta,L} \cdot \ln N)$	Field tests 2 static 2 cyclic	3,173–5,017	D = 34 cm L/D = 6.47 = const. h/D = 1.18 = const. $D_r \approx 1.0$	$\alpha_{y,L} = 0.085$ $t_{y,L} = 0.125$ $\alpha_{\theta,L} = 0.060$ $t_{\theta,L} = 0.080$
Truong et al. (2019)	$y_N = y_1 \cdot N^{\alpha_{y,T}}$	Centrifuge 3 static 14 cyclic	50–1,500	D = 1.1 cm & 4 cm L/D = 11.4 & 6 h/D = 2 & 3 D_r = 0.57 - 0.95	$\alpha_{y,T} = (0.3 - 0.22D_r)[1.2(1 - \zeta_c^2)(1 - 0.3\zeta_c)]$
Li et al. (2020)	$y_N = y_1 \cdot N^{T_{b,L} \cdot T_{c,L}}$	Centrifuge 2 static 18 cyclic	42–153	D = 1.8 cm L/D = 5 = const. h/D = 8 D_r = 0.5 & D_r = 0.8	$T_{b,L}(\zeta_b) = 0.07335$ $T_{c,L}(\zeta_c, D_r = 0.8) = -1.707(\zeta_c + 0.31)^2 + 0.949$ $T_{c,L}(\zeta_c, D_r = 0.5) = -1.14(\zeta_c + 0.323)^2 + 1.263$

[a] T_b and T_c functions fitted based on the graphical representations given in LeBlanc et al. (2010a).

[b] Polynomial factors for the determination of: T_c ($\zeta_c \leq -0.3$): a = 113.33; b = 288.56; c = 238.88; d = 73.48; e = 9.94.
T_c ($\zeta_c > -0.3$): a = 3.06; b = −6.50; c = 5.22; d = −2.76; e = 0.99.

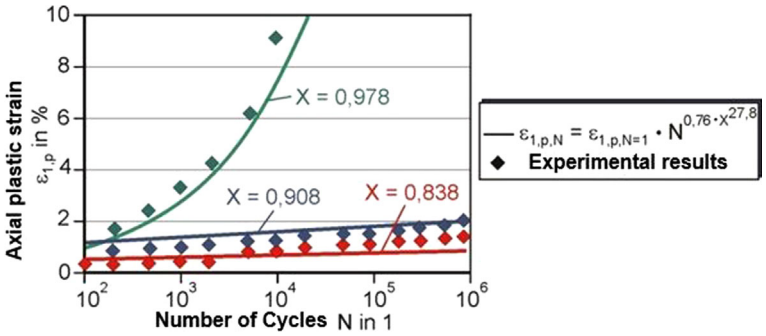

FIGURE 2 Results of a cyclic triaxial compression test and formulation evaluation after Huurman (1996).[16]

with

$$\tilde{A}_{cyc} = r_A \cdot \left(3 - 1.143 \cdot \frac{z}{D}\right) + 0.343 \cdot z/D \tag{3}$$

Here r_A is a factor depending on the load cycle number. For the static case, $r_A = 1$ applies, for $N = 100$ $r_A = 0.3$ and for $N = 10^5$ $r_A = 0$. This modification yields p-y curves that depend on the actual number of load cycles.

Recently, Song et al.[13] proposed an 'overlay model' that transfers an arbitrary static p-y curve to a cycle p-y curve for a given number of cycles using y-multipliers. This overlay model is derived based on the Stiffness Degradation Method (SDM) introduced in Section 2.2.

2.2 | The stiffness degradation method

The stiffness degradation method (SDM) presented in[5] and[6] is a simplified explicit method that concentrates on the practical feasibility, with the purpose of keeping the number of required input parameters as small as possible. The SDM is built based on the elasto-plastic constitutive law of Mohr-Coulomb's perfect plasticity with the stress-dependent stiffness after Ohde[14]:

$$E_s = \kappa \cdot \sigma_{at} \cdot \left(\frac{\sigma_m}{\sigma_{at}}\right)^{\lambda} \tag{4}$$

Here, E_s represents the oedometric stiffness of the soil and σ_m the mean normal stress. σ_{at} is the reference stress equal to 100 kPa. The parameters κ and λ describe the stress-dependency of the soil stiffness, which for non-cohesive soils can be estimated through semi-empirical values depending on the relative density, for example, after EAU (2012).[15]

The governing equation of the SDM is the semi-empirical equation after Huurman[16] which describes the increase of axial strains in a cyclic triaxial compression test (cf. Figure 2):

$$\frac{\varepsilon^a_{cp,N}}{\varepsilon^a_{cp,N=1}} = N^{b_1(X)^{b_2}} \tag{5}$$

Here $\varepsilon^a_{cp,N=1}$ is the axial strain after the first loading, and $\varepsilon^a_{cp,N}$, the axial strain after N-th loading. N is the cycle number, b_1 and b_2 are regression parameters mathematically derived from a series of cyclic consolidated drained triaxial tests (CD). The parameter X is interpreted as the cyclic stress ratio and characterises the load intensity relative to failure stress.

$$X = \frac{\sigma_1}{\sigma_{1f}} = \frac{\sigma_1}{\sigma_3 \cdot \frac{1+\sin\varphi}{1-\sin\varphi} + c \cdot \frac{2\cos\varphi}{1-\sin\varphi}} \tag{6}$$

σ_1 is the maximum stress under cyclic loading in axial direction, and σ_{1f} represents the static failure stress, which can be expressed in terms of c, φ, and confining stress σ_3.

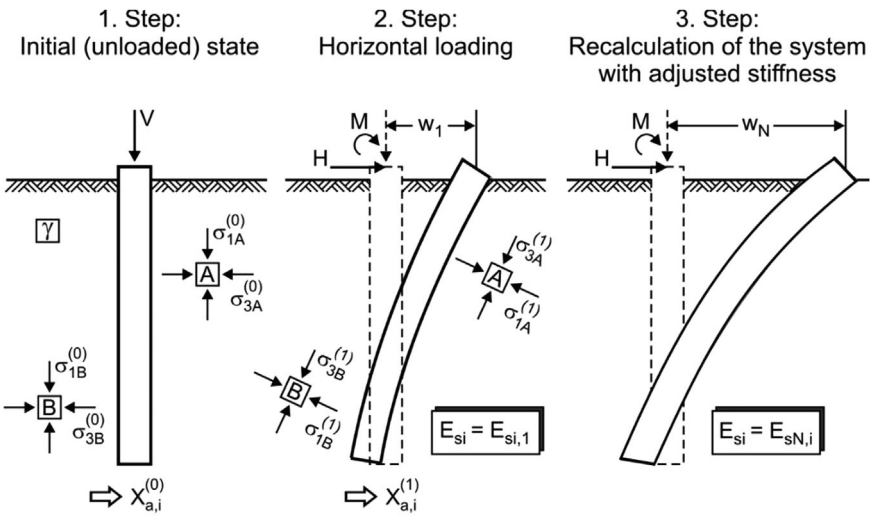

FIGURE 3 The computation procedure of SDM.[5]

Huurman's semi-empirical equation describes the deformation of a soil element under constant load intensity. In the SDM, Huurman's equation is numerically translated indirectly through the degradation of elastic soil stiffness:

$$\frac{\varepsilon^{a}_{cp,N=1}}{\varepsilon^{a}_{cp,N}} = \frac{E_{s,N}}{E_{s,1}} = N^{-b_1 X^{b_2}} \tag{7}$$

By assigning different degraded soil stiffnesses to the elements of the system and repeating the numerical simulation, an interaction of adjacent elements during cyclic loading and a stress redistribution in the system is accounted for. The regression parameters b_1 and b_2 are dependent on both the type of a sand and its relative density and must in general be determined by a series of triaxial tests. Typical ranges of these parameters are reported in Achmus et al.[5] and also Albiker.[6] According to literature, the b_1 varies from 0.10 up to 0.30, while b_2 varies from 0.50 to 20.0. Based on literature review and additional results of cyclic triaxial testing, Albiker[6] concluded that with regard to b_1 and b_2, the type of a sand is much less important than the relative density. For medium dense sand, he proposed $b_1 = 0.15$ and $b_2 = 0.5$, and for dense sand the proposed values were $b_1 = 0.12$ and $b_2 = 0.5$.

A problem with the utilisation of Huurman's equation for the pile-soil system is that in a system the principal stress axes rotate during loading and both the minor principal stress σ_3 and the major principal stress σ_1 change. Moreover, the initial stress state before application of the cyclic load portion is in general anisotropic, which means that cyclic stress ratios before and after load application $X^{(0)}$ and $X^{(1)}$ must be distinguished, which refer to different failure stresses. Therefore, a characteristic stress ratio X_C is defined, which substitutes the X-value in Equation 7. This ratio describes the difference between cyclic stress ratios in the initial step $X^{(0)}$ and the cyclic stress ratio in the loading step $X^{(1)}$ regarding the maximal difference between $X^{(0)}$ and $X^{(1)}$. In this way, the cyclic load intensity is redefined as follows:

$$X_C = \frac{X^{(1)} - X^{(0)}}{X^{(1)}_{max} - X^{(0)}} = \frac{X^{(1)} - X^{(0)}}{1 - X^{(0)}} \tag{8}$$

For one-way cyclic loaded monopiles, the SDM procedure is carried out in three steps (see Figure 3):

1. Initial step: the initial soil stresses and the dead loads are applied to compute the $X^{(0)}$ values on every stress point in the numerical model.
2. First loading with cyclic load: the cyclic loads are applied as static loads in the system to compute the values of $X^{(1)}$ on each stress point. Furthermore, the degraded elastic soil stiffness is computed according to $X^{(0)}$, $X^{(1)}$, and the given parameters b_1, b_2, c and φ with respect to the considered cycle number N.
3. Cyclic loading with degraded soil stiffness: new calculations are carried out with the same loading scenario and the degraded elastic soil stiffness with respect to the required cycle number exported from the second step. Precisely, it means that, in this step, a constant but non-homogenous soil stiffness is used. For each cycle number to be considered, a separate new calculation is required.

TABLE 2 The input parameters for the comparison computation between SDM and CSAM in accordance with.[5,6].

Relative density	κ[–]	λ[–]	c[kPa]	φ[°]	ψ[°]	ν[–]	b_1[–]	b_2[–]
Medium dense	400	0.60	0.1	35.0	5.0	0.25	0.15	0.5
Dense	600	0.55	0.1	37.5	7.5	0.25	0.12	0.5

In the SDM procedure, the first two steps are implicit, serving to compute the variables for the third explicit step. With these steps, the cyclic deformation is computed indirectly through the degraded elastic soil stiffness.

2.3 | Discussion of approaches

Among the introduced approaches, the semi-empirical approaches and cyclic p-y curve methods are mostly used in practical design for their simple application and satisfying computational efficiency. A major disadvantage of the two approaches is the inaccurate consideration of the soil-pile interaction. Besides, the available cyclic p-y curves are partially not experimentally validated or validated for only small cycle numbers.

The Stiffness Degradation Method (SDM), as a simplified numerical method focuses on the practical feasibility instead of theoretical accuracy; thus, requires only eight input parameters (see Table 2). With the more realistic modelling of the soil structure interaction and consideration of site-specific soil conditions compared with the semi-empirical approaches and p-y curves, the computation accuracy with SDM is much improved.

However, the SDM has its weakness due to its indirect numerical translation, that is, the indirect generation of cyclic deformation through degradation of the elastic soil stiffness. This procedure is programming-friendly and convergence-friendly but limits its further application as it is only compatible with a constitutive law, in which the deformation mainly depends on one parameter (the oedometric stiffness modulus). In more advanced constitutive laws, such as the Hypoplasticity model[17] or the Hardening Soil Small Strain model,[18] the deformation depends on several interacting parameters, which makes the application of the SDM very difficult or even impossible.

Since the Stiffness Degradation Method (SDM) cannot be applied in combination with general sophisticated constitutive laws, it has no potential for further development and optimisation. For instance, applications to the problem of a cyclic eccentrically loaded footing showed that with the simple constitutive law used in the SDM a realistic prediction of the tilting of the footing under monotonic load is not possible. Therefore, a new numerical explicit method is proposed that overcomes the weakness of SDM, and at the same time, keeps the practical feasibility of the SDM.

3 | THE NEW NUMERICAL METHOD

In the new method, Huurman's semi-empirical equation[16] still serves as the basic governing equation (see Equation 5), but the numerical application procedure is modified. Since the weakness of SDM is mainly caused by the indirect numerical application of Huurman's equation, in the new numerical method, the cyclic deformation is generated by directly applying strain to the soil elements on stress integration points. In other words, the term $N^{b_1(X)^{b_2}}$ does not serve as a reduction factor for soil stiffness, but as a strain amplifier to describe the cyclic effect based on the strains computed from the monotonic loading. Due to the proposed numerical procedure, the new numerical method is termed 'Cyclic Strain Accumulation Method' and abbreviated as CSAM.

Since the cyclic deformation in CSAM is generated by directly applying strains on stress integration points, it is compatible with arbitrary static constitutive laws, and the form of strain application can be modified easily. In the current version of CSAM, the cyclic strain accumulation due to the cyclic normal loading following a triaxial compression stress path is considered (by applying Huurman's equation). If necessary, other strain accumulation mechanisms, such as the shear strain accumulation due to cyclic direct shearing, can also be taken into account under the framework of CSAM. In general, the CSAM provides a highly flexible framework and thus shows great potential for further modification and optimisation.

3.1 | The first version of CSAM

In the first version of CSAM, the computation conditions are similar to the SDM: This means it utilised Mohr-Coulomb constitutive law with perfect plasticity, and the stress state, which serves for the derivation of the strain increase rate, is also read from the first (virgin) loading path. The mechanical effect of the SDM through the soil stiffness degradation can be illustrated by Hooke's law and the Huurman equation (see Equations 5 and 7) as

$$\varepsilon_{ii,N} = \frac{1}{E_N}[\sigma_{ii} - \nu(\sigma_{jj} + \sigma_{kk})] = \frac{1}{E_1/N^{b_1(X)^{b_2}}}[\sigma_{ii} - \nu(\sigma_{jj} + \sigma_{kk})] = N^{b_1(X)^{b_2}}\varepsilon_{ii,N=1} \tag{9}$$

$$\gamma_{ij,N} = \frac{1}{G_N}\tau_{ij} = \frac{1}{G_1/N^{b_1(X)^{b_2}}}\tau_{ij} = N^{b_1(X)^{b_2}}\gamma_{ij,N=1} \tag{10}$$

Here the subscripts i, j, k stand for the coordinates x, y, z.

From Equations 9 and 10, it is clear that all six cartesian strain components are amplified through the degraded soil stiffness. To achieve the same mechanical effect as the SDM, in the first version of CSAM, all six Cartesian strains are amplified directly with the same amplifier $N^{b_1(X)^{b_2}}$ without using the soil stiffness as the transfer medium:

$$\varepsilon_{ii,N} = N^{b_1(X)^{b_2}} \cdot \varepsilon_{ii,N=1} \Rightarrow \Delta\varepsilon_{ii,N} = \left(N^{b_1(X)^{b_2}} - 1\right) \cdot \varepsilon_{ii,N=1} \tag{11}$$

$$\gamma_{ij,N} = N^{b_1(X)^{b_2}} \cdot \gamma_{ij,N=1} \Rightarrow \Delta\gamma_{ij,N} = \left(N^{b_1(X)^{b_2}} - 1\right) \cdot \gamma_{ij,N=1} \tag{12}$$

With these equations, the additional strains induced by cyclic loading can be calculated dependent on the load cycle number N for each stress point (Gaussian point) of the FE model. In the numerical model, these additional strains are applied and considered, in the same way, as temperature or creep strains. Whereas in the SDM, the cyclic deformation is generated 'indirectly', in the CSAM, it is generated 'directly', as will be discussed with a computation example later.

Like the SDM, the numerical procedure of CSAM in the first version is carried out in three steps. In the first two steps, the characteristic stress ratio X_c is calculated from the stress conditions, and the applied cyclic strains with respect to different cycle numbers calculated using Equations 11 and 12. In the third step, cyclic strains are applied directly in the numerical model. Depending on the expected cycle numbers, the third step can be divided into several substeps. In other words, to compute the cyclic behaviour with CSAM, only one computation with a stepwise increase of strains is required, which is computationally more efficient than the SDM, where the cyclic deformation for each cycle number requires a separate new calculation.

To validate the CSAM, first, two typical monopile geometries in accordance with the examples from Achmus et al.[5] are investigated (see Figure 4), which are subjected to a one-way load with complete unloading of 15.0 MN and the corresponding lever arm to pile head (at the soil surface) of 20.0 m.

Regarding soil parameters, Mohr-Coulomb's perfect plasticity and stress-dependency on soil stiffness after Equation 4 are kept. The friction coefficient μ between the monopile and soil is assumed as $\mu = 2/3\tan\varphi$. The two regression parameters b_1 and b_2 for soil cyclic behaviour are not adopted from Achmus et al.[5] but taken from the experimental work done by Albiker[6] and are considered to be more accurate than the mathematical average values from Achmus et al.[5] The utilised soil parameters are summarised in Table 2.

Under the above-mentioned conditions, calculations were done to compare SDM and CSAM using the Finite Element Software ABAQUS.[19] A 3D-model with 8-noded brick elements (C3D8) is used to examine the behaviour of the monopile in sandy soil under cyclic lateral loading conditions. Due to symmetry in loading and geometry, only half of the system was examined. The monopile was modelled as open-ended pile. After setting the initial stresses in the soil by means of a k_0-procedure, the pile's steel elements were inserted by a 'wished in place'-procedure, which means that the effects of the installation procedure on the soil around the pile was neglected. The contact interaction between the monopile and adjacent soil elements was simulated with a penalty method applying Coulomb's friction law.

Regarding the size of the model domain and the number and size of the elements, a sensitivity study was conducted. The chosen model dimensions of a width 14-times the pile diameter and a depth of twice the pile length ensure that the calculation results are not affected by the boundary conditions. A typical finite element mesh chosen for a reference system is depicted in Figure 4.

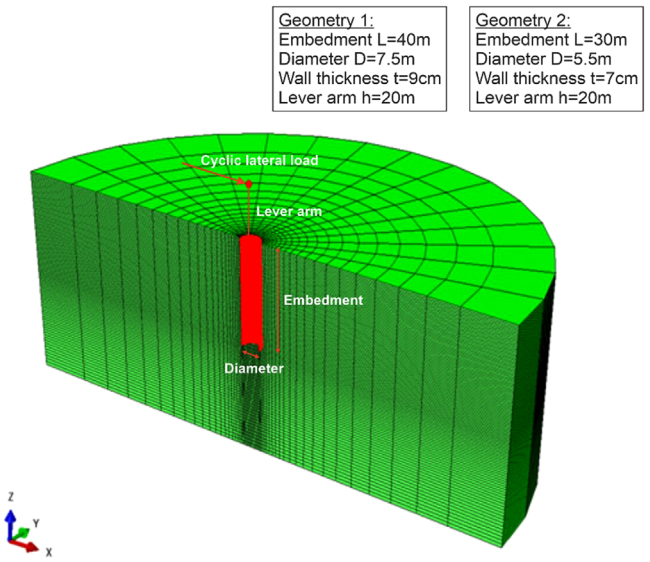

FIGURE 4 The used ABAQUS model.

The results are illustrated in terms of deflection curves and pile head displacement in Figures 5–7. Figure 5 shows deflection lines for a monopile with D = 7.5 m and L = 40 m under maximal loading after different load cycles, as calculated for SDM and CSAM. As expected, the head displacement of the monopile increases with the number of load cycles, and the rotation point of the pile moves slightly downwards both for the medium dense (Figure 5A) and dense sand (Figure 5B). A good agreement between the results from SDM and CSAM is detected. The SDM predicts slightly greater deflections than the CSAM. This slight difference is caused by the different numerical procedures for applying semi-empirical equations in the system (see Equations 9–12). Due to the assignment of different stiffness reductions for each element in the system in SDM, a redistribution of stresses compared to the monotonic loading case occurs. Also, in CSAM, stress redistributions occur due to the assignment of different volume strains to the soil elements. However, the CSAM reaches the cyclic stress state under a different loading path. The cyclic deformation is generated by 'directly' applying strains on soils, whereas in SDM, the cyclic deformation is generated 'indirectly' by reducing the soil stiffness. Therefore, a perfect agreement cannot be expected. However, for a monopile system, the differences in cyclic behaviour are obviously rather small.

As a second example, deflection lines for a monopile with D = 5.5 m and L = 30 m are considered. The same maximum load (H_{max} = 15 MN) with the same lever arm with respect to the soil surface (h = 20 m) was applied, which means that the relative load magnitude for this system is considerably higher than in the first example. Consequently, greater deflections and a more pronounced cyclic accumulation of displacements result. For this case, the CSAM and SDM results are almost the same.

Figure 7 shows the pile head displacements extracted from Figures 5 and 6 as a function of the number of load cycles. Evidently, the agreement between CSAM and SDM in the pile head displacement can be considered satisfying. Thus, it can be concluded that for monopiles under cyclic lateral loading (which is the system the SDM was developed for), CSAM gives approximately the same results as SDM when the same material law of the soil is applied.

3.2 | Variation of constitutive law and consideration of un- and reloading stress path

Next, in this study, under the framework of CSAM, the influence of constitutive law on cyclic behaviour is investigated by comparing the cyclic behaviour using the constitutive laws of Mohr-Coulomb's perfect plasticity (MC) and Hypoplasticity with intergranular strain (Hypo), respectively. Furthermore, the effect of considering the un- and reloading stress path during cyclic loading in contrast to considering only the virgin loading stress path (as in the original SDM) is investigated.

The constitutive theory of Hypoplasticity arose from the attempt to capture the soil behaviour in a mathematical structure as simple as possible. It is distinctive in that the main characteristics of the mechanical behaviour of granular material are expressed in one single tensorial equation. It differs from elasto-plastic models in that the splitting of the deformation into an elastic and a plastic part no longer occurs, and neither do the mathematical constructs such as plastic potential,

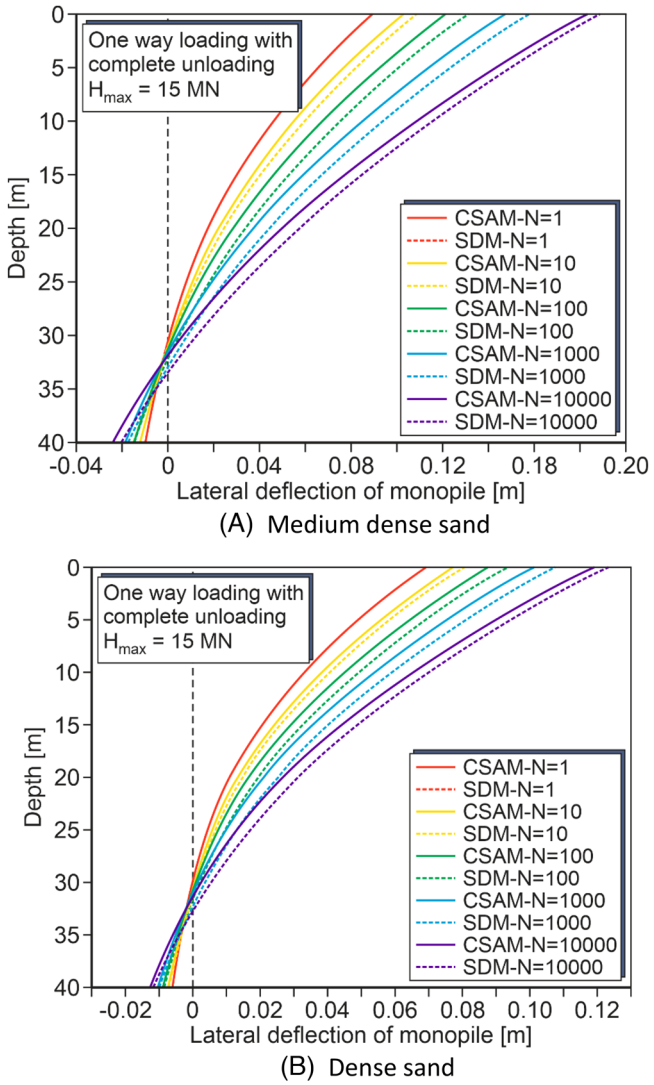

FIGURE 5 Pile deflection curves using CSAM and SDM for the pile embedment length L = 40 m and pile diameter D = 7.5 m. (A) Medium dense sand. (B) Dense sand.

yield surface, flow rule and consistency condition. In the constitutive law, the influence of the pressure level and the relative density (void ratio) on the soil behaviour or granular materials is taken into consideration. Stiffness, shearing dilatancy or contractancy, and peak friction result from the current void ratio and stress conditions of the soil elements and from the direction of the soil deformation. The theoretical basis and deduction of the hypoplastic relationship are described in detail in.[20,21,22,23]

Under the triaxial stress path and oedometric stress path, the comparison of static soil response using Mohr-Coulomb's perfect plasticity model and the Hypoplasticity model with intergranular strain are illustrated in Figure 8. It can be observed that the soil response using the two constitutive laws is quite different, especially the Mohr-Coulomb model with perfect plasticity could not reproduce the typical hardening behaviour of soils and the difference in un- and reloading and virgin loading paths, which causes inaccuracy in calculating deformation.

For an explicit method, as applied here, an essential requirement to compute the cyclic deformation is an accurate representation of the stress changes in a load cycle. When the plasticity is taken into account in the system, a considerable stress redistribution occurs during the primary loading, especially when using constitutive law like Hypoplasticity with intergranular strain, which can describe the hardening of soil and distinguish the static soil response in the primary and reloading path. In other words, the stress condition at the primary loading occurs only once in the system; therefore, the stress at the reloading path should be more representative than at the primary loading. Due to the stated reason, in the

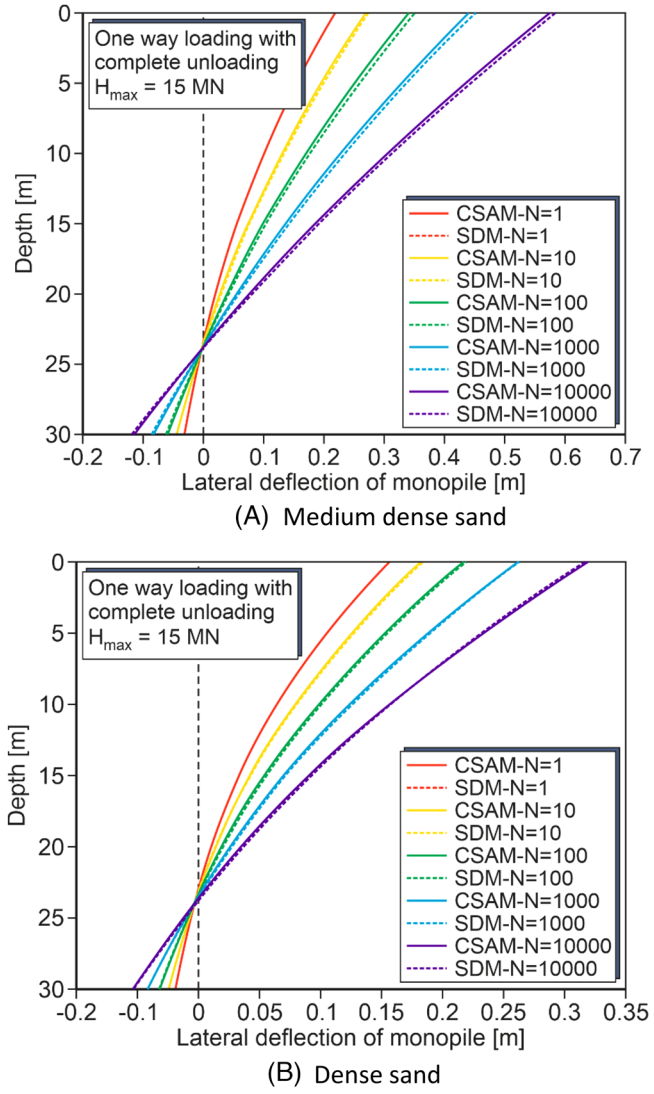

FIGURE 6 Pile deflection curves using CSAM and SDM for the pile embedment length L = 30 m and pile diameter D = 5.5 m. (A) Medium dense sand. (B) Dense sand.

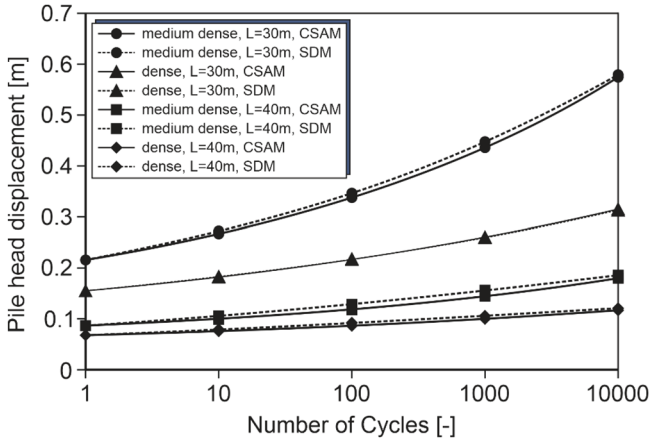

FIGURE 7 The comparison of pile head displacement between SDM and CSAM for two different monopile geometries (L = 30 m/D = 5.5 m and L = 40 m/D = 7.5 m).

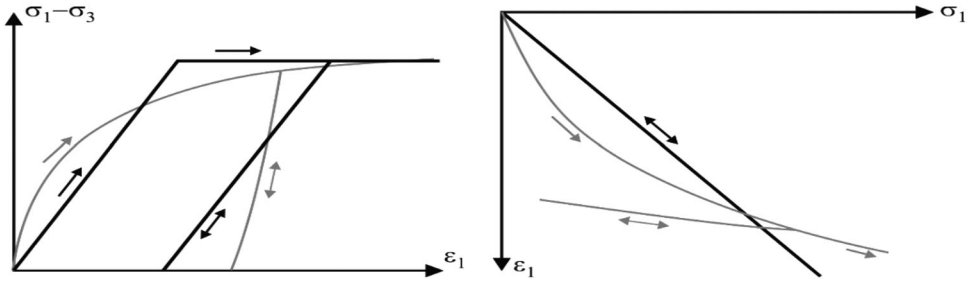

FIGURE 8 Loading and unloading cycles according to linear-elastic ideal-plastic material laws (black lines) and according to Hypoplasticity with intergranular strain (light-grey lines) in the triaxial compression (left) and oedometric stress path (right) (schematic).[24]

TABLE 3 The input parameters for the cyclic computation using Hypoplasticity model with intergranular strain (taken from Wichtmann et al.[26]).

Relative density	φ_c [°]	h_s [MPa]	n [–]	α [–]	β [–]	e_0 [–]	e_{i0} [–]	$e_{c0[-]}$	e_{d0} [–]	R [–]	m_T [–]	m_R [–]	β_R [–]	χ [–]
0.58 (Medium dense)	33.1	4000	0.27	0.14	2.5	0.90	1.212	1.054	0.677	10^{-4}	1.1	2.2	0.1	5.5
0.89 (Dense)	33.1	4000	0.27	0.14	2.5	0.735	1.212	1.054	0.677	10^{-4}	1.1	2.2	0.1	5.5

TABLE 4 The input parameters for the cyclic computation using Mohr-Coulomb perfect plasticity.

Relative density	κ [–]	λ [–]	c [kPa]	φ [°]	ψ [°]	ν [–]
0.58 (Medium dense)	550	0.6	0.1	34.0	4.0	0.25
0.89 (Dense)	900	0.55	0.1	40.0	10.0	0.25

following computation, a further variation is added to distinguish whether the stress state for explicit computation is taken from the primary or reloading path.

The used Hypoplasticity model with intergranular strain was implemented in ABAQUS in terms of User Material (UMAT) provided by Tamagnini et al.[25] The corresponding input parameters are listed in Table 3, taken from Wichtmann et al.[26] for Karlsruhe fine sand. In this study, the basic model conditions in Figure 5 are kept. Medium dense sand and dense sand are again considered with relative densities I_D of 0.58 and 0.89, respectively.

The two cyclic input parameters b_1 and b_2 for the two relative densities are also adopted from Table 2. Besides, the geometry and loading conditions are kept according to Figure 4 (geometry 1, i.e., D = 7.5 m, L = 40 m). The input parameters for the case using Mohr-Coulomb with perfect plasticity are summarised in Table 4. For this investigation, the shear parameters c and φ for the Mohr-Coulomb failure criterion were calibrated such that in a static triaxial compression test, the same failure stress applies as calculated with the Hypoplasticity model with intergranular strain. With the derived φ value, the friction coefficients between the monopile and soil are still assumed as $\mu = 2/3 \tan \varphi$ for all cases. The stiffness parameters κ and λ were adjusted such that under the considered load of H = 15 MN in the static case ($N = 1$), the same pile head displacements occur as for the case with the hypoplastic material law (see Figure 9). This parameter choice enables an easy comparison of the differences between the model approaches regarding the cyclic behaviour of the monopile. As can be seen in Figure 9, this procedure leads to slightly different displacements at smaller loads, where the hypoplastic material law predicts slightly stiffer system behaviour.

3.3 | Consideration of the UN- and reloading stress path

To illustrate the influence of the stress path on the cyclic behaviour, the behaviour of the monopile under cyclic loads using Mohr-Coulomb perfect plasticity was investigated. The stress states used to calculate the characteristic stress ratio X_c (see Equations 6 and 8) were read from the primary stress path and reloading stress path in two cases, respectively.

For the case of medium dense sand, Figure 10 shows the distributions of the characteristic stress ratios. Slight differences can be seen, but in the most important passive region in front of the pile the distributions are quite similar. It might thus be expected that the effect of un- and reloading consideration is not too great.

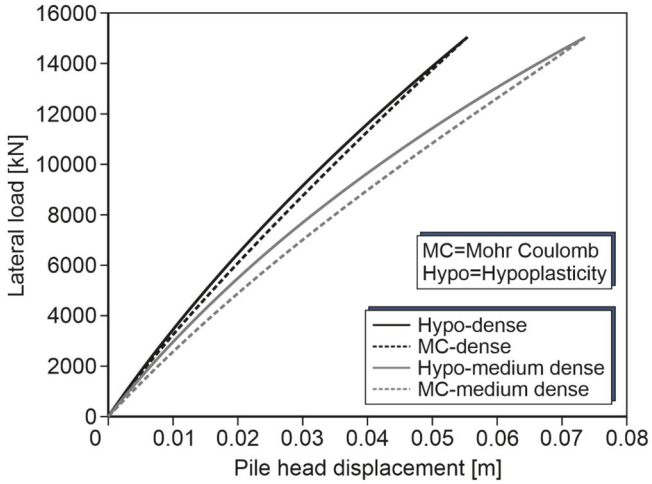

FIGURE 9 Comparison of load-displacement curves of the monopile D = 7.5 m/L = 40 m for the cases with hypoplastic and Mohr-Coulomb material laws.

Figure 11 shows the calculated monopile deflection lines for both medium dense and dense sand, and Figure 13 shows the development of pile head displacements dependent on load cycle number. It is found that considering the more realistic cyclic stress path, that is, the reloading stress path, leads to slightly less accumulation rate of cyclic displacements. For the case of medium dense sand, the static head displacement increased by a factor of 2.33 when reading the stress states from the primary stress path, whereas with consideration of un- and reloading, the increase factor is 2.07. For the case of dense sand, the factors are 1.97 and 1.78, respectively. This shows that the consideration of un- and reloading has a significant effect and should be accounted for. Therefore, in the hypoplastic material law, which distinguishes between virgin loading and reloading behaviour, the un- and reloading states are considered in determining the cyclic stress level X_C.

3.4 | Results for the hypoplastic material law

For the effect of different material laws on the cyclic behaviour of a monopile, the results of calculations using the Mohr-Coulomb and Hypoplasticity material laws are presented in Figure 12. For both material laws, the un- and reloading stress states were considered. The results clearly show that application of the more sophisticated material law does not enhance deviations. In medium dense sand, the MC material law gives slightly greater accumulated displacements than the Hypo material law, while for dense sand, almost identical cyclic displacement increases are obtained.

The comparison of pile head displacements in Figure 13 summarises the gained results. The results of the monopile system analysed confirmed the argument that the CSAM is compatible with arbitrary material law. In addition to being independent of material law, the CSAM produces the same results when the system behaviours after the first loading are identical. Besides, the investigation results show that the stress states after un- and reloading should be considered in determining a representative cyclic stress level.

4 | DISCUSSION

For the monopile systems investigated in Section 3, it comes out that the application of the new CSAM method leads only to marginal deviations from the results gained with the SDM. However, this finding applies only to the investigated monopile systems and cannot be generalised. The SDM is not suitable for systems, in which the target value is the deformation in vertical direction, that is, in direction of gravity. Due to the applied degradation of stiffness, also deformations induced by the (non-cyclic) gravity loads are obtained, which is not intended and leads to an overestimation of accumulated settlements.

As an example, Figure 14 shows the results of SDM and CSAM calculations for the case of a vertical loaded strip footing. The footing dimensions and the loading conditions were taken from a centrifuge test reported by Helm et al. (2000)[27] (also described in Wichtmann et al. 2005)[28]. The results of the test are also depicted in the figure, although the material

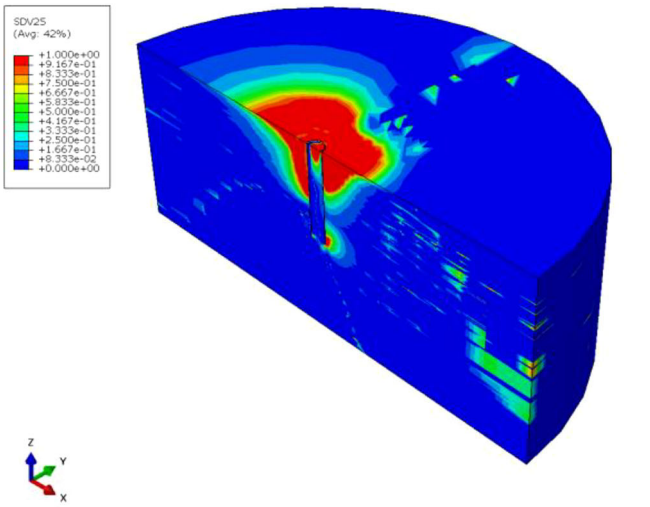

(A) without consideration of un-and reloading

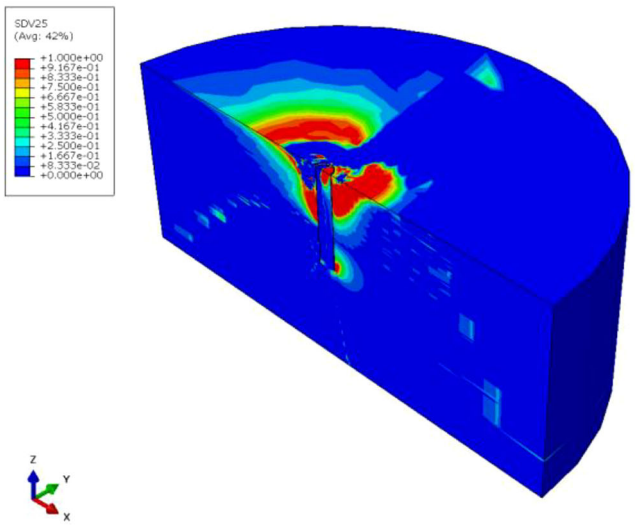

(B) with consideration of un-and reloading

FIGURE 10 Comparison of X_c distributions for medium dense sand using Mohr-Coulomb (MC). (A) Without consideration of un-and reloading. (B) With consideration of un-and reloading.

parameters of the sand were not adapted to the soil conditions in the test. Instead, the parameters for medium dense sand given in the Tables 3 and 4 were applied.

Evidently, the CSAM predicts significantly smaller accumulated settlements than the SDM. The monotonic settlement must of course be identical and is 2.6 cm in the considered case. However, after 10,000 cycles, the CSAM predicts a settlement of 4.6 cm, whereas the SDM predicts 7.1 cm. In the centrifuge test, the monotonic settlement was 2.4 cm and after 10,000 cycles, 5.0 cm was measured. Although no real back-calculation of the centrifuge test was intended here, the comparison shows that the CSAM prediction in this case is—as to be expected—more realistic than the SDM prediction.

5 | SUMMARY AND OUTLOOK

With the basic concept of Stiffness Degradation Method (SDM) after Achmus et al.,[5] a new numerical explicit method termed Cyclic Strain Accumulation Method (CSAM) is proposed for computing the cyclic behaviour of cyclically loaded foundations. The essential difference between SDM and CSAM lies in the numerical procedure; whereas, in the SDM, the

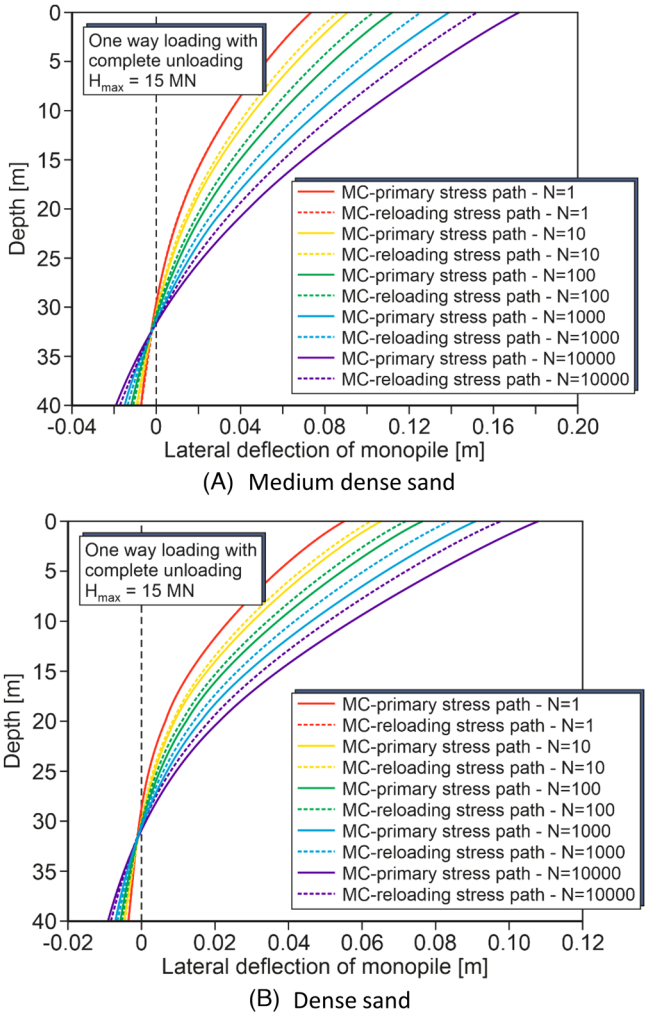

FIGURE 11 Comparison of pile deflection curves using Mohr-Coulomb (MC) with and without consideration of un- and reloading. (A) Medium dense sand. (B) Dense sand.

cyclic deformation is 'indirectly' generated through the degradation of elastic soil stiffness, in the CSAM, the cyclic deformation is generated 'directly' by applying strains to the soil in the system. With this slight modification, some weaknesses of the SDM can be overcome. More advanced material laws that simulate soil behaviour more accurate can be applied in CSAM, and makes possible a more realistic consideration of the cyclic stress paths in the system, consisting of un- and reloading. Besides, CSAM keeps the advantage of practical feasibility of the SDM, and it is even computationally more efficient since in the cyclic stage of the procedure, only one computation with stepwise increase of strains is required, whereas, in SDM, for the cyclic deformation of each cycle number, a separate new computation is required.

From the results for a monopile system presented in this paper, the following main conclusions can be drawn:

- For the monopile systems considered, the CSAM predicts similar deflections to the SDM. Since it has been shown that the SDM predicts reasonable results for monopiles in sands,[5,6,7,8,9] this conclusion can also be transferred to the CSAM.
- The consideration of un- and reloading in the determination of the cyclic stress level in the elements of the system leads to a smaller cyclic displacement accumulation. Therefore, un- and reloading stress states should be taken into account in predicting cyclic displacements.
- The calculations of the simple MC material law and the sophisticated Hypo material law lead only to marginal deviations. Obviously, the choice of the material law does not considerably affect the prediction of the cyclic performance of the system.

The newly developed CSAM offers the possibility to investigate the cyclic behaviour not only of monopiles, but also of other foundation structures (e.g., gravity foundations), which transfer cyclic loads to the subsoil by vertical cyclic stresses.

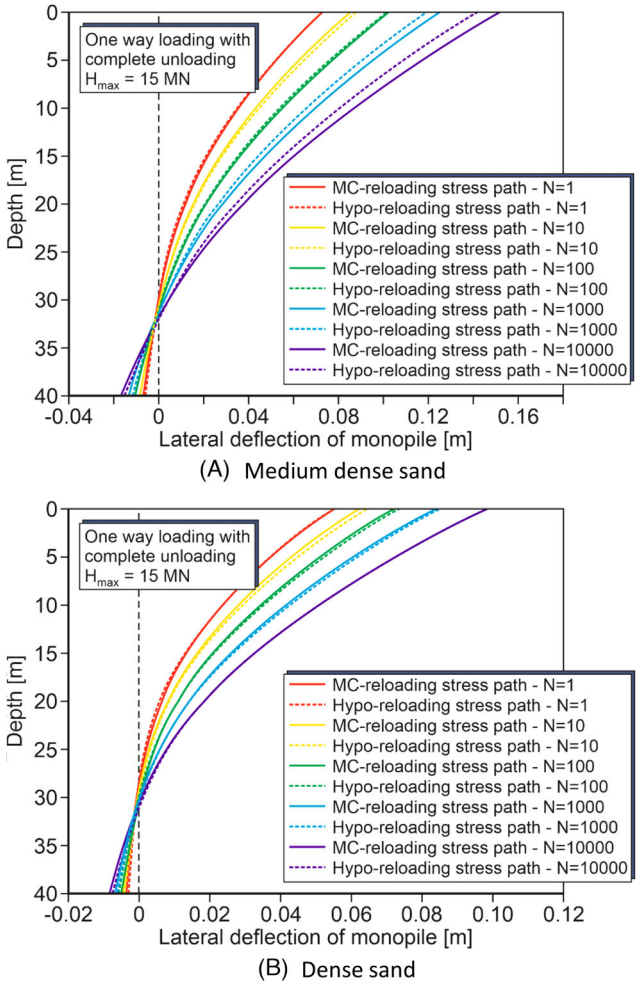

FIGURE 12 Comparison of pile deflection curves using Mohr-Coulomb (MC) and Hypoplasticity with consideration of un- and reloading. (C) Medium dense sand. (D) Dense sand.

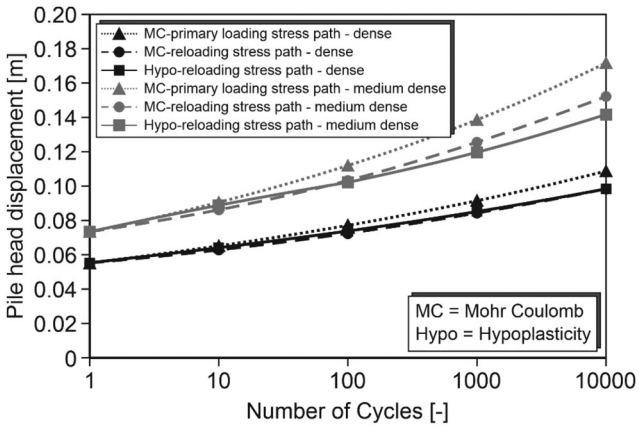

FIGURE 13 The comparison of pile head displacement between Mohr-Coulomb (MC) and Hypoplasticity (hypo).

This is not suitable with the SDM since the stiffness degradation leads to increased deformations due to the vertical acting initial (static) stresses. Moreover, other stress conditions affecting the accumulation of cyclic strains (for instance, cyclic oedometric compression) can be easily incorporated into CSAM by adding additional cyclic strains. The SDM and CSAM have been used to predict the settlement of a strip footing under cyclic vertical loading. The numerical results show that CSAM gives more realistic results compared to SDM.

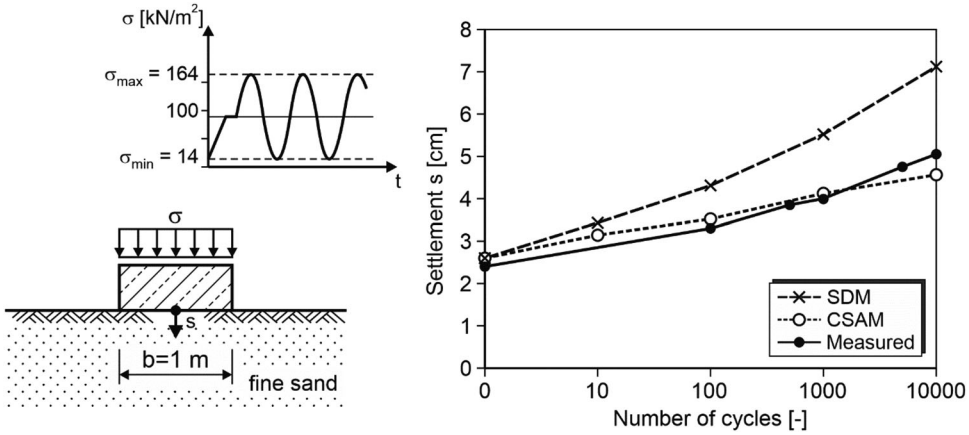

FIGURE 14 Comparison of CSAM and SDM predictions for a cyclically vertical loaded circular footing.[27,28]

It should be noted that CSAM as well as SDM are simplified explicit models targeted to estimate the increase of deformations of a geotechnical system due to cyclic loading. The models presuppose drained loading conditions and a constant cyclic load intensity during application of the cyclic loads, which might not be suitable for certain systems and loading conditions. Despite these limitations, it is concluded that the CSAM is a very promising new numerical method to account for the cyclic deformation of foundations.

ACKNOWLEDGEMENTS

Open access funding enabled and organized by Projekt DEAL.

DATA AVAILABILITY STATEMENT

The data that support the findings of this study are available on request from the corresponding author.

ORCID

Shuhan Cao https://orcid.org/0000-0002-8234-5947
Khalid Abdel-Rahman https://orcid.org/0000-0002-8385-7258

REFERENCES

1. Dafalias YF, Manzari MT. Simple plasticity sand model accounting for fabric change effects. *J Eng Mech*. 2004;130(6):622-634.
2. Liu H, Diambra A, Abell JA, Pisanò F. Memory-enhanced plasticity modeling of sand behavior under undrained cyclic loading. *J Geotech Geoenviron Eng*. 2020;146(11):04020122.
3. Niemunis A, Wichtmann T, Triantafyllidis T. A high-cycle accumulation model for sand. *Comput Geotech*. 2005;32(4):245-263.
4. Wichtmann T, Machaček J, Zachert H, Günther H. Validierung eines hochzyklischen Akkumulationsmodells anhand von Modellversuchen und Messungen an realen Bauwerken. *Bautechnik*. 2019;96(2):160-175. (in German).
5. Achmus M, Kuo YS, Abdel-Rahman K. Behavior of monopile foundations under cyclic lateral load. *Comput Geotech*. 2009;36(5):725-735.
6. Albiker J. *Untersuchungen zum Tragverhalten zyklisch lateral belasteter Pfähle in nichtbindigen Böden, Heft 77*. Institut für Geotechnik, Leibniz Universität Hannover (PhD thesis, in German); 2016.
7. Westermann K, Zachert H, Wichtmann T. Vergleich von Ansätzen zur Prognose der Langzeitverformungen von OWEA-Monopilegründungen in Sand: teil 1: grundlagen der Ansätze und Parameterkalibration. *Bautechnik*. 2014;91(5):309-323. (in German).
8. Westermann K, Zachert H, Wichtmann T. Vergleich von Ansätzen zur Prognose der Langzeitverformungen von OWEA-Monopilegründungen in Sand: teil 2: simulationen und Schlussfolgerungen. *Bautechnik*. 2014;91(5):324-332. (in German).
9. Yang M, Luo R, Li W. Numerical study on accumulated deformation of laterally loaded monopiles used by offshore wind turbine. *Bull Eng Geol Environ*. 2018;77(3):911-921.
10. Frick D, Achmus M. A model test study on the parameters affecting the cyclic lateral response of monopile foundations for offshore wind turbines embedded in non-cohesive soils. *Wind Energy Science*. 2022;7(4):1399-1419.
11. API. *Recommended Practice 2GEO-Geotechnical and Foundation Design Considerations*. American Petroleum. Institute, Version October 2014; 2014.
12. Dührkop JVol. 20. *Zum Einfluss von Aufweitungen und zyklischen Lasten auf das Verformungsverhalten lateral beanspruchter Pfähle in Sand*. Vol. 20. Institut für Geotechnik und Baubetrieb, Technische Universität Hamburg-Harburg (PhD thesis, in German); 2009.

13. Song J, Achmus M. Derivation of cyclic p-y curves for the design of monopiles in sand. Paper Ref: SEMC 2022/249. The Eighth International Conference on Structural Engineering, Mechanics and Computation, SEMC, Cape Town, South Africa; 2021. September 2022. (accepted for publication).
14. Ohde J. Zur Theorie der Druckverteilung im Baugrund. *Der Bauingenieur*. 1939;20:S451-S459. (in German).
15. *Recommendations of the Committee for Waterfront Structures Harbours and Waterways (EAU)*. 11th ed. German Geotechnical Society; 2012.
16. Huurman M. Development of traffic induced permanent strains in concrete block pavements. *Heron*. 1996;41(1):29-52.
17. Wu W. *Hypoplastizität als mathematisches Modell zum mechanischen Verhalten granularer Stoffe*. Veröffentlichungen des Instituts für Bodenmechanik und Felsmechanik der Universität Karlsruhe Heft 139 (in German); 1992.
18. Benz T. *Small-Strain Stiffness of Soils and its Numerical Consequences*. Universität Stuttgart, Institut für Geotechnik; 2007.
19. Dafalias Y. F., Manzari M. T.. *ABAQUS User's Manual 2020*. Simulia. The publication year is June 2004.
20. Bauer E. Calibration of a comprehensive constitution equation. *Soils Found*. 1996;36(1):13-26.
21. Gudehus G. A comprehensive constitution equation for granular materials. *Soils Found*. 1996;36(1):1-12.
22. Kolymbas D. *Ein nichtlineares viskoplastisches Stoffgesetz für Böden*. Veröffentlichungen des Instituts für Bodenmechanik und Felsmechanik der Universität Karlsruhe; 1977. Heft 77 (in German).
23. von Wolffersdorf PA. *Verformungsprognosen für Stützkonstruktionen* Heft 141 (in German). Veröffentlichungen des Instituts für Bodenmechanik und Felsmechanik der Universität Karlsruhe; 1997.
24. EANG. Empfehlungen des Arbeitskreises Numerik in der Geotechnik –EANG, 1. Auflage, Deutsche Gesellschaft für Geotechnik e.V (In German). 2014.
25. Tamagnini C, Sellari E, Masin D, von Wolffersdorff PA. 2009. https://soilmodels.com/download/plaxis-umat-hypoplas-zip/
26. Wichtmann T, Triantafyllidis T. An experimental database for the development, calibration and verification of constitutive models for sand with focus to cyclic loading: part I – tests with monotonic loading and stress cycles. *Acta Geotech*. 2016;11(4):739-761.
27. Helm J, Laue J, Triantafyllidis T. Untersuchungen an der RUB zur Verformungsentwicklung von Böden unter zyklischen Belastungen. *Workshop Boden unter fast zyklischer Belastung*. Schriftenreihe des Instituts für Grundbau und Bodenmechanik der Ruhr-Universität Bochum; 2000. Heft Nr. 32.
28. Wichtmann T, Niemunis A, Triantafyllidis T. FE-Prognose der Setzung von Flachgründungen auf Sand unter zyklischer Belastung. *Bautechnik*. 2005;82(12):902-911. (in German).

How to cite this article: Cao S, Abdel-Rahman K, Achmus M. A new method for the analysis of foundation behavior in sand under drained high-cycle loading. *Int J Numer Anal Methods Geomech*. 2023;47:1876–1893. https://doi.org/10.1002/nag.3542